RF INJECTOR BEAM DYNAMICS OPTIMIZATION AND INJECTED BEAM ENERGY CONSTRAINTS FOR LCLS-II*

C. Mitchell†, F. Sannibale, H. Qian, J. Qiang, M. Venturini, LBNL, Berkeley, CA 94720, USA
F. Zhou, J. Schmerge, P. Emma, T. Raubenheimer, SLAC, Menlo Park, CA 94025, USA

Abstract

LCLS-II is a proposed high-repetition rate (>1 MHz) Free Electron Laser (FEL) X-ray light source, based on a CW superconducting linac, to be built at SLAC National Accelerator Laboratory. The injector technology is based on a high-repetition rate RF photoinjector gun developed as part of the Advanced Photoinjector Experiment (APEX) at Lawrence Berkeley National Laboratory. Exploration of the injector design settings is performed using a multiobjective genetic optimizer to optimize the beam quality at the injector exit (~100 MeV). In this paper, we describe the current status of LCLS-II injector design optimization, with a focus on the sensitivity of the optimized solutions to the beam energy at the injector exit, which is constrained by the requirements of the downstream laser heater system.

INTRODUCTION

The LCLS-II project is an upgrade to the existing LCLS X-ray free electron laser (FEL) at SLAC National Accelerator Laboratory, designed to provide photons between 200 eV and 5 keV at repetition rates up to 1 MHz using a CW superconducting linac [1, 2]. To meet these requirements, the injector must deliver a sequence of high-brightness electron bunches at ~1 MHz for 20 pC, 100 pC (nominal), or 300 pC charge. The beam will be produced using an RF photogun based on the gun design at APEX [3], with acceleration to ~100 MeV using eight 9-cell superconducting cavities. An RF buncher is used to provide ballistic bunching before acceleration.

A simplified schematic of the injector front-end is shown in Fig. 1. To explore the injector settings, a multi-objective genetic optimizer was previously developed using the codes NSGA-II and ASTRA [4]- [5]. In this paper, we update these optimization results to include recent changes to the injector design [6]. In addition to changes in the layout, RF buncher, and solenoid design, the injector is now nominally operated with RF cavities 2 and 3 powered off, allowing the first RF cavity to play a role similar to a traditional capture cavity to improve emittance compensation. This results in a trade-off between the final beam energy and optimized injector performance near the nominal beam energy of 100 MeV, which we explore.

OPTIMIZATION PROCEDURE

Details regarding the optimization procedure and simulation parameters have been described elsewhere [4]- [5]. The two objectives to be minimized are the transverse emittance of the beam and the bunch length at the injector exit. Table 1 shows the parameters that are varied during optimization. A phase of 0 denotes the phase of maximum acceleration, while a phase of -90° denotes zero crossing. In each ASTRA simulation, the transverse laser pulse shape at the cathode is a Gaussian distribution truncated at a radius of $1\sigma_x$, and the laser pulse longitudinal shape is a plateau with rise and fall time of 2 ps. The initial momentum distribution of the beam is generated by assuming a conservative value for the thermal emittance coefficient at the cathode of 1 mm-mrad/mm, with a corresponding initial beam energy spread. During optimization, several constraints are imposed on the beam at the injector exit to satisfy the requirements of the downstream beam transport and FEL systems [5].

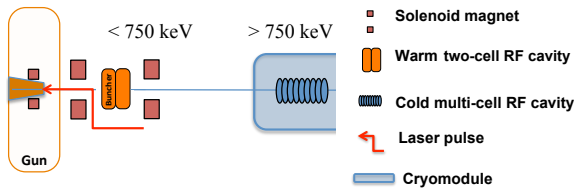

Figure 1: Primary components in the low-energy portion of the injector system for LCLS-II. The cryomodule contains 8 standard 9-cell 1.3 GHz superconducting cavities (only the first is shown).

Table 1: Set of 10 Parameters Varied During Injector Optimization

Parameter	Range
Gun phase	[-15,15] deg
Buncher field	[0,2.1] MV/m
Buncher phase	[-90,-40] m
Solenoid 1 & 2 fields	[0.01,0.1] T
Cavity 1 field	[10,30] MV/m
Cavity 4 field	[0,32] MV/m
Cavity 4 phase	[-15,15] deg
RMS spot size at the cathode	[0.05,5] mm
Bunch length at the cathode	[5,75] ps

Figure 2 shows the Pareto front of optimized solutions for each of the three bunch charge values of 20, 100, and 300 pC. Each simulation within Astra is performed using 10K simulation particles, so the emittance values shown are

* Work supported by the U.S. Department of Energy under Contract Nos. DE-AC02-76SF00515, DE-AC02-05CH11231, and the LCLS-II Project.
† ChadMitchell@lbl.gov

ISBN 978-3-95450-147-2

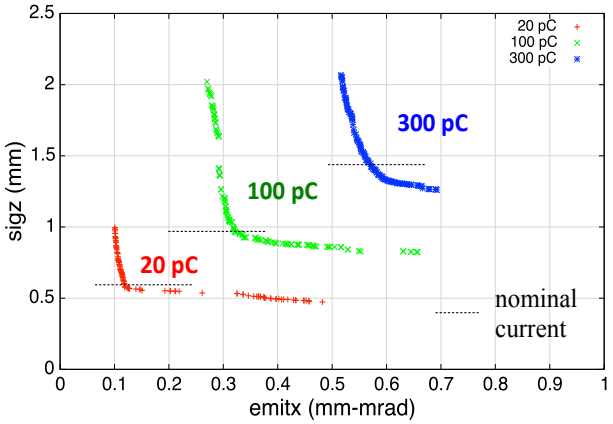

Figure 2: Pareto-optimal fronts illustrating the performance of the LCLS-II injector system at 20, 100, and 300 pC bunch charge.

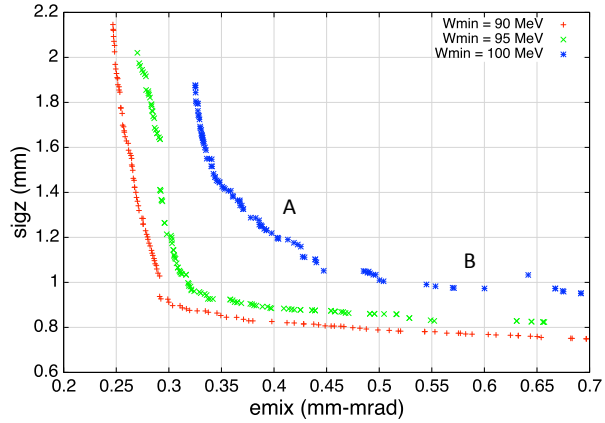

Figure 3: Pareto-optimal fronts for 100 pC charge illustrating the sensitivity of emittance and bunch length to the value of the constraint placed on the final beam energy.

slightly overestimated due to numerical noise, especially at high charge. The emittance values obtained at higher resolution (100K particles) for solutions near the nominal current are 0.10, 0.29, and 0.49 μm for the three charge states, respectively.

Requirements of the Laser Heater System

After exiting the 8-cavity cryomodule, the beam enters a laser heater (LH) system. The laser heater is a well-established method to control the microbunching instability by artificially increasing the beam slice-energy spread σ_E [7]. In LCLS-II, it consists of a 0.54 m undulator placed in the middle of a weak 4-dipole chicane and a $\lambda_L = 1030$ nm laser. For a fixed undulator period and a fixed laser wavelength, the laser peak power P_L required to achieve the desired σ_E increases as the electron beam energy is reduced [8]. To avoid exceeding constraints on the laser power $P_L < 0.35$ MW, we impose a lower bound of 95 MeV on the beam kinetic energy at the injector exit. In addition, to accomodate the dispersion of the LH chicane, the beam projected energy spread must be limited to < 1%. We impose the more conservative constraint that it be < 200 keV.

CONSEQUENCES OF THE BEAM ENERGY CONSTRAINT

During optimization, a constraint of the form $W \geq W_{\min}$ is applied, where W denotes the beam kinetic energy at the injector exit. Fig. 3 compares the 100 pC Pareto fronts that are obtained for the cases when $W_{\min} = 90$, 95, and 100 MeV, demonstrating that the choice of energy constraint has a significant effect on the injector performance. We examine this effect near regions A and B shown in the figure.

Letting ΔW_j $(j = 1, \ldots, N)$ denote the energy gain in each of the N active accelerating cavities, we must have:

$$\sum_{j=1}^{N} \Delta W_j \geq W_{\min}, \qquad \Delta W_j \leq \Delta W_{\max}, \tag{1}$$

where $\Delta W_{\max}$ is the maximum possible energy gain per cavity. The two conditions (1) imply that there is a minimum energy gain required in cavity j (for $j = 1, \ldots, N$):

$$qE_{\rm acc}L_{\rm acc}\cos\phi \geq W_{\min} - (N-1)\Delta W_{\max}. \tag{2}$$

In (2) we have assumed that $\Delta W_j = qE_{\rm acc}L_{\rm acc}\cos\phi$, where $E_{\rm acc}$ is the cavity's average accelerating gradient, $L_{\rm acc}$ is the cavity length, and ϕ is the cavity RF phase. Equality is possible in (2) only if all of the remaining $N-1$ cavities $(k \neq j)$ are operated on-crest with $\Delta W_k = \Delta W_{\max}$.

It follows from (2) that the range of acceptable accelerating gradient and phase for each cavity decreases as the energy constraint $W_{\min}$ increases. For example, for a standard 9-cell TESLA cavity, $L_{\rm acc} = 1.038$ m and $E_{\rm acc} = E_0/2$, where E_0 is the on-axis field amplitude given in Table 1 [9]. We require that $E_{\rm acc} \leq 16$ MV/m, for which simulation gives a maximum on-crest energy gain of $\Delta W_{\max} = 17.44$ MeV. As a result, with cavities 2 and 3 powered off and $W_{\min} = 100$ MeV, (2) implies that the minimum possible field amplitude E_0 in any cavity is 23.5 MV/m (when the cavity is run on-crest).

Emittance Compensation

To minimize space-charge induced projected emittance growth, the beam is typically matched onto an invariant envelope to ensure damped emittance oscillations [10]. In the case of a split photoinjector based on a standing wave linac, this gives the following matching conditions at the entrance to the first RF accelerating cavity [10]- [11]:

$$\sigma'_{x,y} = 0, \qquad \sigma_{x,y} = \frac{2}{\gamma'}\left[\frac{I_{pk}\langle g\rangle}{3\gamma I_A}\right]^{1/2}, \tag{3}$$

where $\gamma' = (eE_{\rm acc}/mc^2)\cos\phi$. Here $I_A = 17.054$ kA is the Alfven current, I_{pk} is the beam peak current, and $\langle g\rangle \sim 1$ is a geometrical factor that depends on the longitudinal beam profile.

Consider a 100 pC beam entering the first accelerating cavity at the nominal beam energy of 750 keV. To achieve the

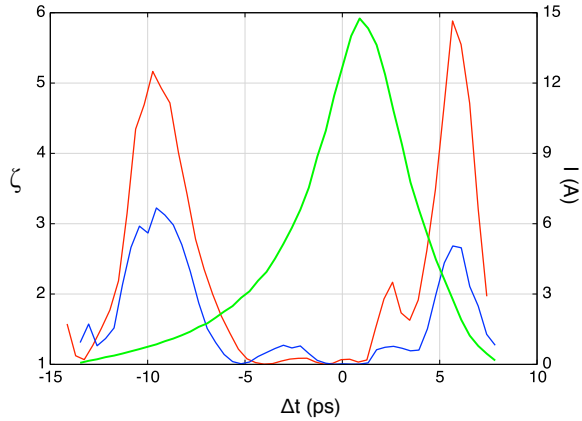

Figure 4: Slice mismatch parameter ζ along the length of the bunch for two well-optimized solutions with final energies of 95 MeV (blue) and 100 MeV (red). The final current profile is similar in the two cases (green).

nominal current of 12 A at the injector exit, (3) implies that $\gamma'\sigma_{x,y} \leq 0.0195$ at the entrance to the first cavity. Solutions near the nominal current (region A of Fig. 3) have transverse beam sizes of 1.5 mm or greater at the cavity entrance; to achieve smaller beam size requires excessive focusing in the second solenoid. Thus, emittance compensation (3) requires a field amplitude in the first cavity less than 13.3 MV/m if the cavity is run on-crest, which (2) indicates cannot be achieved for an energy constraint $W_{\min} > 94.1$ MeV. As a result, we expect the space-charge contribution to the projected emittance for those optimized solutions in region A to become large when the applied energy constraint exceeds this value.

To illustrate this, Fig. 4 shows the slice mismatch parameter $\zeta = (\gamma\beta_0 - 2\alpha\alpha_0 + \beta\gamma_0)/2$ along the length of the bunch for two optimized solutions at the injector exit with final energies of 95 MeV and 100 MeV, respectively, showing that superior slice-to-slice matching is possible at lower energy.

Longitudinal Compression

After capture of an electron bunch from the RF gun, longitudinal compression may occur in several stages. First, ballistic bunching occurs in the drift region between the RF buncher and the first accelerating cavity. The resulting compression factor is determined by the buncher voltage and frequency, the gun voltage, and the length of the drift region. For those solutions near region B in Fig. 3, the buncher is run at near the maximum voltage to achieve maximum compression, and all three parameters may be assumed fixed.

Second, velocity bunching may occur in the accelerating cavities, which requires running one or more of the cavities off-crest to introduce an energy-bunch length correlation along the bunch. Neglecting the backward-propagating RF wave in the accelerating structures, an approximate expression for the compression due to velocity bunching in any cavity is given by [12]:

$$C = \cos\phi_f \left(\cos\phi_i - \frac{h}{2\alpha k\gamma_i}\right)^{-1}, \quad (4)$$

where $\phi_i = kz - \omega t + \phi_0$ is the RF phase seen by a reference particle at the cavity entrance, γ_i is the relativistic gamma at the cavity entrance, $k = \omega/c$ is the RF wavenumber, and $\alpha = eE_{\rm acc}/mc^2k$ is a dimensionless measure of the cavity gradient. Here h is a measure of the relative energy chirp along the length of the bunch at the cavity entrance, and

$$\phi_f \approx \sin^{-1}\left[\sin\phi_i - \frac{1}{2\alpha\gamma_i}\right]. \quad (5)$$

With the first cavity run at low gradient, the range of phase values available for any cavity is restricted due to the energy constraint (1), severely limiting the velocity compression that can be achieved. For example, for those 100 MeV solutions shown in Fig. 3, the largest off-crest phase value of any cavity is $\phi_i = 10°$. If such a cavity is run with $E_{\rm acc} = 16$ MV/m and $h \approx 0$, then (4) implies at most a 1.5% reduction in bunch length due to velocity compression.

CONCLUSION

This work describes optimization of the LCLS-II injector system after including recent changes in the layout, RF buncher, and solenoid design, in an operating mode with cavities 2 and 3 powered off. While these changes have resulted in a significant improvement in injector performance [6], operating in this mode introduces a conflict between the final beam quality (emittance and bunch length) and the final beam energy. Operating with a beam energy near 95 MeV is expected to provide acceptable beam performance while limiting the burden on the downstream laser heater system.

ACKNOWLEDGEMENT

This work is supported by the Office of Science of the U.S. Department of Energy under Contract Numbers DE-AC02-76SF00515, DE-AC02-05CH11231, and the LCLS-II Project, and made use of computer resources at the National Energy Research Scientific Computing Center.

REFERENCES

[1] The LCLS-II Collaboration, "The LCLS-II Conceptual Design Report," Technical report, 2013.

[2] T. Raubenheimer, Proc. FEL2015, Daejeon, Korea, WEP014 (2015).

[3] F. Sannibale *et al*, Proc. FEL2015, Daejeon, Korea, MOP024 (2015).

[4] C. Papadopoulos *et al*, Proc. FEL2014, Basel, Switzerland, THP057 (2014); SLAC-PUB-16210.

[5] C. Papadopoulos *et al*, Proc. IPAC2014, Dresden, Germany, WEPRO015 (2014).

[6] F. Zhou *et al*, Proc. FEL2015, Daejeon, Korea, MOP021 (2015).

ISBN 978-3-95450-147-2

[7] Z. Huang *et al*, Phys. Rev. ST Accel. Beams **7**, 074401 (2004).

[8] M. Venturini and Z. Huang, LCLS-II TN-14-05 (2014).

[9] B. Aune *et al*, Phys. Rev. ST Accel. Beams **3**, 092001 (2000).

[10] L. Serafini and J. Rosenzweig, Phys. Rev. E **55**, 7565 (1997).

[11] M. Ferrario *et al*, SLAC-PUB-8400 (2000).

[12] S. G. Anderson *al*, Phys. Rev. ST Accel. Beams **8**, 014401 (2005).